Digest Journal of Nanomaterials and Biostructures Vol. 9, No. 2, April - June 2014, p. 721 - 737

SPIN WAVES IN SYSTEMS WITH VARIABLE SIZE, DIMENSIONALITY AND DIFFERENT CRYSTAL STRUCTURES: EFFECTS IN THE MAGNETIZATION DEPENDENCE ON TEMPERATURE

N. Radutoiu, C. M. Teodorescu •
National Institute of Materials Physics, P.O. Box MG-7, 077125 Bucharest-Magurele, Romania

Monte-Carlo estimations of the integrals of Bose-Einstein distribution function for magnons are performed, by avoiding number of approximations involved in the usual derivation of the Bloch $T^{3/2}$ law, describing the dependence of magnetization with temperature in the low temperature regime, where the main mechanism of magnetization decrease is due to spin waves. More precisely: (i) the magnon dispersion law is considered the exact one (depending on the crystal structure) and not the quadratic approximation $\varepsilon(k)$ α k^2; (ii) the integrals are performed over the first Brillouin zone and the limit of the integral is not extended to infinity; (iii) the dimensionality of the system is taken into account: 1D, 2D and 3D systems are considered; (iv) finite size magnetic systems are treated by rigorous summation of the Bose-Einstein distribution function, without using the continuous limit. The results can be summarized as follows: (a) Infinite three-dimensional (3D) systems exhibit deviations from the Bloch $T^{3/2}$ law, namely the deviation from zero Kelvin magnetization $|\Delta M|/M(0)$ behaves as T^{γ}, where γ is sensibly (by some 10 %) larger than 3/2 and, also, depends on the crystal structure considered. (b) Finite 3D systems exhibit more drastic deviation from the Bloch law, in that the γ exponent deviates seriously from 3/2, going up to 2.5 for small systems of about 1,000 atoms. (d) Finite 2D systems also show serious deviations from the Bloch-like T law. As described a few years ago [C.M. Teodorescu, Surf. Sci. **601**, 4292 (2007)], finite temperature magnetization may be considered only in finite size 2D systems. Several recent examples from literature are analyzed in the framework of the actual theoretical results. It is shown that $M(T)$ analysis in the low temperature regime allows one to extract the average nanoparticle size of the magnetic moieties, and as well the exchange interaction and average spin quantum number.

(Received April 22, 2014; Accepted May 23, 2014)

Keywords: Spin waves; Nanoparticles; Low-dimensional systems; Monte-Carlo simulations

1. Introduction

The Bloch $T^{3/2}$ law is perhaps one of the most known and useful derivations from the theory of magnetism [1]. The usual Curie-Weiss phenomenological theory of ferromagnetism was found unsatisfactory in the low temperature regime. Instead, the dependence of magnetization with temperature $M(T)$ was explained by introducing the spin waves (magnons), which are bosons propagating into the ferromagnetic crystal, described by wavevectors $\boldsymbol{k}$. The $T^{3/2}$ dependence is obtained from the integral over the magnon states of the Bose-Einstein distribution; in three-dimensional (3D) systems, the integral over the k space of $k^2 dk$ pulls out a $T^{3/2}$ factor, once the energy of magnons is proportional to k^2. It follows that for low dimensionality systems the temperature exponent should be equal to 1 for 2D systems, and to 1/2 for 1D magnetic system.

However, the 2D integral over magnon states exhibits a logarithmic divergence in the origin ($k = 0$), and the 1D integral exhibits an algebraic divergence at $k = 0$. This can be connected

• Corresponding author: teodorescu@infim.ro

to the Mermin-Wagner theorem [2] which states that no long range magnetic order may be achieved for systems with dimensions lower than 3 at finite temperatures. Gibbs energy calculations at finite fields and temperatures yielded a similar result [3], but here the divergence occurs when the applied field is set to zero. Moreover, applying the Dyson-Maleev formalism [4,5], many-loop corrections proposed by Ref. [3] reinforced the divergence for the 1D case.

Nevertheless, linear $M(T)$ dependencies on the form $M(T) = M(0)$ - *Const.* x T were reported for quasi-2D systems synthesized by molecular beam epitaxy (MBE) [6-9] or even under-linear dependencies $M(T) = M(0)$ - *Const.* x T^{γ}, with $\gamma < 1$ in Ref. [10]. Some years ago, Ref. [6], based also on experimental results on Ni single atomic layers grown on Cu(001), suggested that a consistent 2D spin wave theory can be elaborated only for finite size 2D systems, where the introduction of a low cutoff $k_{\text{min.}}$ wavevector of magnons avoids the divergence near the origin of the k space for 2D Bose integrals. This low cutoff magnon wavevector is connected to the inverse of the maximum magnon wavelength, which, in turn, is connected to the finite size of the 2D system investigated. Consequently, the analysis of $M(T)$ in the low temperature regime can be used to estimate both the dimensionality (from the value of the temperature exponent) and the size (from the value of the multiplication constant) of finite size magnetic systems, such as: (i) buried or embedded 2D layers or 3D nanoparticles; (ii) 3D nanoparticles whose size does not allow their observation by structural methods, e.g. X-ray diffraction or electron microscopy.

It is now needed a further step in the development of this physics, namely the evaluation of the effects of the low wavevector cutoff also in 3D systems of variable crystal structures. But, in dealing with this evaluation one encounters the following problem: the low cutoff magnon wavevector is not that low (in 3D) such as to permit the quadratic approximation of the magnons' dispersion law. Indeed, for a 1D system, the magnon dispersion law can be written as $\varepsilon(k) = 4JS[1-\cos(ka)] \approx 2JS(ka)^2$, which holds for $ka << 1$ (here and in the following a is the lattice constant, J the Heisenberg exchange integral, and S the individual spin value; for 2D and for 3D systems with different crystal structures the reader is reported to the following Section). Now, for a maximum magnon wavelength of $\lambda_{max} = 10\ a$, the cutoff value $k_{min} = 2\pi / \lambda_{max}$ and $k_{min}a = \pi/5$, which is not a small value. Back to 3D systems, $\lambda_{max} = 10\ a$ corresponds to nanoparticles of 1,000 atoms, whose lateral dimensions range between 2 and 3 nm, so to real systems of interest for this study. A 2D system composed by a similar number of spins will have $\lambda_{max} = 1000^{1/2}\ a \approx 32\ a$ and $k_{min}a = \pi/16$, which starts to be acceptably small. For a 1D system, $k_{min}a = \pi/500$ and the quadratic approximation holds perfectly. Therefore, especially for 3D finite systems the quadratic dispersion law for magnons is not appropriate.

For larger systems (ribbon-shaped Fe nanoparticles with typical dimensions from several tens to hundreds of nanometers), computations were performed by keeping all the approximations from the spin wave theory in Ref. [11], where just the Bose integral was splitted into different parts, where more 1D, 2D, or 3D magnons' degrees of freedom are identified according to the magnons' wavelength which could be accommodated just over the length of the ribbons (1D), the length x width (2D), or length x width x thickness (3D). In this pioneering work, however, no special meaning was given e.g. to the necessity of introduction of a cutoff in 2D or 1D systems, besides which the Bose integrals are divergent.

The problem of finite size ferromagnets and deviations from the Bloch law was treated for finite cubic systems a few years ago in Ref. [12], where, by using summation instead of integration and the exact magnon dispersion law instead of the parabolic approximation, a dependence such as $M(T) = M_0$ - Const.$_1$ x $T^{3/2}$ + Const.$_2$ x T. However, the author agrees also with the fact that in some experimental cases the modified Bloch law $M(T) = M(0)$ - *Const.* x T^{γ} reproduces with equal accuracy some experimental data. Therefore, more effort is needed, in particular comparisons with experimental data and tackle of other crystal structures, in order to provide more insight in the low temperature behavior of magnetization in finite size effect. As stated above, this effort is supplemented in the present paper by a treatment of 2D and 1D cases, which may present nonvanishing average magnetic moment at finite temperatures only when their size is finite.

Section 2 will summarize in more details the usual derivation of the Bloch law. It will be shown that is highly desirable to achieve accurate evaluations of the Bose sums or integrals with as

few as possible approximations. This is the reason for which a first development of this paper (§ 3.1) deals with numerical computation of the Bose integrals without (i) the quadratic approximation of the magnons' dispersion law; (ii) without extending the Bose integral to infinity, but performing real integration over the magnon states over the first Brillouin zone. This will be achieved for 3D systems of simple cubic (*sc*), face-centered cubic (*fcc*) and body-centered cubic (*bcc*) systems. Indeed, deviations of the temperature exponent from 3/2 are found, which are depending on the crystal structure considered. Then, in the same Paragraph, evaluation of the sums of Bose-Einstein distribution function with real dispersion laws will be performed and compared with the integrals for infinite systems. The results will be found to be strong dependent on the size of the system, but also the dependence on the crystal structure is noticeable for finite systems.

§ 3.2. deals with computations on finite size 2D systems and is, in fact, a more accurate continuation of Ref. [6]. § 3.3. presents briefly the 1D case, whereas Section 4 is concerned with the experimental data. In this Section, some comments will be made connected to the observability of the phenomena predicted in this paper in real experiments and then five cases of interest of surface magnetism will be analyzed. Finally, Sec. 5 presents the conclusions.

2. Approximations in the usual derivation of spin waves' induced magnetization dependence

In Appendix 1, the first steps of the derivation from [1] are recalled, including the first approximation used (Ap1), that of small oscillation amplitudes of the spins. It is clear that theoretical effort is also needed to deal with non-small amplitude spin waves, where several magnon modes have to be taken into account [13]. However, this first approximation will not be questioned in this paper.

Approximation Ap1: *Small oscillation amplitudes*
The dispersion law for magnons is derived in the linear case as:
(i) 1D system

$$\hbar\omega = 4\,JS\,(1 - \cos ka) \tag{1}$$

For 2D or 3D lattices of spins, the dispersion law is generalized as follows:

$$\hbar\omega = 2JS\left[Q - \sum_{l=1}^{N} \cos\left(\boldsymbol{a}_l \cdot \boldsymbol{k}\right)\right] \tag{2}$$

where the sum is performed over all Q nearest-neighbors separated from the considered spin by the lattice vectors $\boldsymbol{a}_l$, $l = 1,...,Q$.
Examples:
(ii) 2D square lattice :

$$\hbar\omega = 4\,JS\,(2 - \cos k_x a - \cos k_y a) \tag{3}$$

(iii) 3D simple cubic (*sc*) lattice:

$$\hbar\omega = 4\,JS\,(3 - \cos k_x a - \cos k_y a - \cos k_z a\,) \tag{4}$$

(iv) 3D body centered cubic (*bcc*) lattice:

$$\hbar\omega = 16JS\left(1 - \cos\frac{k_x a}{2}\cos\frac{k_y a}{2}\cos\frac{k_z a}{2}\right) \tag{5}$$

(v) 3D face centered cubic (*fcc*) lattice:

$$\hbar\omega = 8JS\left(3 - \cos\frac{k_x a}{2}\cos\frac{k_y a}{2} - \cos\frac{k_y a}{2}\cos\frac{k_z a}{2} - \cos\frac{k_z a}{2}\cos\frac{k_x a}{2}\right) \tag{6}$$

Once the dispersion law is derived, by summing over the magnon states the Bose-Einstein distribution (magnons are bosons, according to Holstein-Primakoff theory [14], even if individual spins may take half integer values), one can derive the relative variation of the magnetization:

$$\frac{|\Delta M|}{M(0)} \equiv \frac{M(0)-M(T)}{M(0)} = \frac{1}{NS}\sum_{\boldsymbol{k}} \frac{1}{\exp\left(\frac{\hbar\omega(\boldsymbol{k})}{k_B T}\right)-1} \tag{7}$$

N being the total number of spins of the system, S the spin quantum number and k_B the Boltzmann constant.

Approximation Ap2: *Small magnon wavevectors*

The product $2JS$ multiplying the magnon's dispersion law is on the order of 10-30 meV for most magnetic systems [1]. On the other hand, the aim of the theory is to explain the magnetic behaviour at low temperatures $T \leq 30$ K, where $k_B T \leq 2.5$ meV. Relevant contributions in the Bose-Einstein distribution law (7) will be given only by small wavevectors magnons. Consequently, the cosine function in all dispersion laws (1-6) is developed in power series over k and only the second order terms in k are retained. The preceding equations yield a quadratic dispersion law for magnons, irrespective on the dimensionality of the system and on the crystal structure (for 1D, 2D and 3D):

$$\hbar\omega = 2\,JS\,(ka)^2 \tag{8}$$

Approximation Ap3: *Large systems and quasicontinuous spectrum of magnons*

As usual in solid state physics, the magnon waves must be stationary within the system, considered either as a rectangular box of dimensions (L_x x L_y x L_z) for 3D systems, as a rectangle (L_x x L_y) for 2D systems or as a line segment of dimension L for 1D systems:

$$k_\alpha L_\alpha = 2\pi n_\alpha,\ \alpha = x, y, z \tag{9}$$

by respecting the dimensionality (r) of the system: $r = 1$ with no α indexing in (9); $r = 2$ with $\alpha = x, y$; or $r = 3$ where (9) holds fully. Hence, the sum over magnon states from (7) is transformed as follows:

$$\sum_{\mathrm{k}} f(\boldsymbol{k}) \equiv \sum_{\mathrm{k}} f(\boldsymbol{k})\Delta^r n = \frac{\prod_{j=1}^{r} L_j}{(2\pi)^r}\sum_{\mathrm{k}} f(\boldsymbol{k})\Delta^r k = \begin{cases} \dfrac{V}{(2\pi)^3}\displaystyle\int f(\boldsymbol{k})d^3k, & \text{for 3D systems} \\ \dfrac{A}{(2\pi)^2}\displaystyle\int f(\boldsymbol{k})d^2k, & \text{for 2D systems} \\ \dfrac{L}{2\pi}\displaystyle\int f(\boldsymbol{k})dk, & \text{for 1D systems} \end{cases} \tag{10}$$

where $1 = \Delta^r n = \Delta n_x \Delta n_y \Delta n_z$ in the 3D case ($r = 3$) and has similar forms in the cases of $r = 1, 2$; the volume of a 3D system is $V = L_x L_y L_z$ and the area of a 2D system is $A = L_x L_y$. The integral(s) over each component a of the magnon wavevector k_α is performed within the first Brillouin zone ($-\pi/a \rightarrow 0 \rightarrow \pi/a$). A necessary comment here is that the zero value of the magnon wavevector corresponds to an infinite magnon wavelength $\lambda = 2\pi/k$; however, this is valid only for infinite spatially extended systems. For real systems, one has to isolate the zero magnon wavevector from the integral in (10) by introducing a low wavevector cutoff $k_{\min.}$ connected to the maximum available wavelength $\lambda_{\max.} = 2\pi/k_{\min.}$; $\lambda_{\max}$ is necessarily connected to the (macroscopic) dimension of the system. As was already commented, this observation will be of particular interest for magnetic clusters and for low dimensional systems with $r \leq 2$, since it avoids the divergence of the Bose-Einstein integrals near the $k = 0$.

Approximation Ap4: *Small lattice constants, small temperatures, large exchange constants: extension of the integral over the first Brillouin zone to infinite reciprocal space*

For computation of the relative variation of the magnetization (7), one has to introduce the Bose-Einstein distribution function $[\exp(\hbar\omega / k_BT) - 1]^{-1}$ into (10). At the edges of the Brilouin zone $k = \pm \pi/a$, $\hbar\omega = 4JSQ \approx 0.1$ - 0.5 eV, whereas $k_BT \approx$ 1-10 meV for the physics of interest. Consequently, at the edges of the Brillouin zone the Bose-Einstein distribution function $[\exp(\hbar\omega / k_BT) - 1]^{-1} \approx \exp(-\hbar\omega / k_BT) \sim 10^{-5}$ at most. In this case, the integral over the first Brillouin zone is extended over the whole reciprocal space, by assuming that large wavevector magnons with $k > \pi/a$ give negligible contribution in the sum over the Bose distribution function.

In view of all the above approximations, one obtains the well-known Bloch $T^{3/2}$ law for infinite 3D systems:

$$\frac{|\Delta M|}{M(0)} = \frac{V}{NS(2\pi)^3}\int_{\mathbf{k}} \frac{d^3k}{\exp\left(\frac{\hbar\omega(\mathbf{k})}{k_BT}\right)-1} = \frac{V}{NS2\pi^2}\int_0^{\pi/a[\to\infty]} \frac{k^2dk}{\exp\left(\frac{2JSa^2k^2}{k_BT}\right)-1} = \frac{1}{4\pi^2SR}\left(\frac{k_BT}{2JS}\right)^{3/2}\int_0^{\infty}\frac{x^{1/2}dx}{e^x-1} \qquad (11)$$

(Ap3) (Ap2) (Ap4)

where $V = Na^3/R$, R being the number of atoms in the elementary cell ($R = 1$ for *sc*, $R = 2$ for *bcc*, $R = 4$ for *fcc*). The vertical arrows in the above equation indicate the level at which each one of the approximations (Ap2-4) appears. In the following, we shall question numerically these approximations and we shall modify the above expression for finite and low-dimensional (1D, 2D) systems.

In fact, this last approximation (Ap4) comprises two approximations: (i) once one integrates over a sphere of radius π/a in the k space instead of the first Brillouin zone, which has its specific shape [1] and this approximation will be denoted as (Ap4.1); (ii) secondly, the integral is extended to infinity, and this approximation will be denoted as (Ap4.2).

3. Computations

3.1. Three dimensional systems. Combined effects of size and crystal structure

In the following, computations will be performed for values of thermal energy k_BT sometimes exceeding the nearest-neighbor direct exchange energy J. The Curie temperature of the corresponding infinite ferromagnet is given by $k_BT_C = S(S + 1)\, J\, z/3$, where z is the number of nearest-neighbors of an interacting spin S in the material [1]. Therefore, for large values of the total atomic spin S (> 1) and $z = 8$ for *bcc* structures or $z = 12$ for *fcc* structures, k_BT_C may exceed the product $S \times J$ by almost one order of magnitude. Although this range of temperatures cannot be regarded as "low" (according to Ap.4 discussed above), it still characterizes a magnetic system where the overall exchange energy aligning each spin by its nearest neighbors is considerably higher than the thermal energy. A complete treatment of this problem would involve also discarding the approximation of small oscillation amplitudes (Ap.1). Nevertheless, e.g. in Ref. [12], a simulation based on a modified Bloch law is proposed for manganese ferrite nanoparticles, up to a maximum temperature of about 300 K, which has the same order of magnitude as the Curie temperature of this compound [15]. Therefore, we will retain simulations where the thermal energy is on the same order of magnitude as the nearest-neighbor exchange energy, knowing that the considered (bulk) systems are still far below their Curie temperatures and, finally, testing these computations with experimental data in Sec. 4. On the other hand, smaller values of the parameter $(k_BT)/(JS)$ will be more often used in the computation (the density of input values will be increased for smaller temperatures), therefore all derivations infered from these computations will be much more sensitive and applicable for low temperatures, where it is to be expected that the spin waves dominate the temperature variation of the magnetization.

The Bose-Einstein 3D integrals:

$$\int_{-\pi/a}^{\pi/a} dk_x \int_{-\pi/a}^{\pi/a} dk_y \int_{-\pi/a}^{\pi/a} dk_z \frac{1}{\exp\left(\frac{\hbar\omega(\boldsymbol{k})}{k_B T}\right)-1}$$

are performed by Monte-Carlo method, by using at least 10^9 summation steps, which correspond to approximately 1,000 integration steps over each direction. The relative variation of the final result during the last Monte-Carlo steps was in the range of 2×10^{-4}. Figure 1 presents the results of the integration for *sc*, *bcc* and *fcc* crystal structures. The data are fitted with a power function (the modified Bloch law):

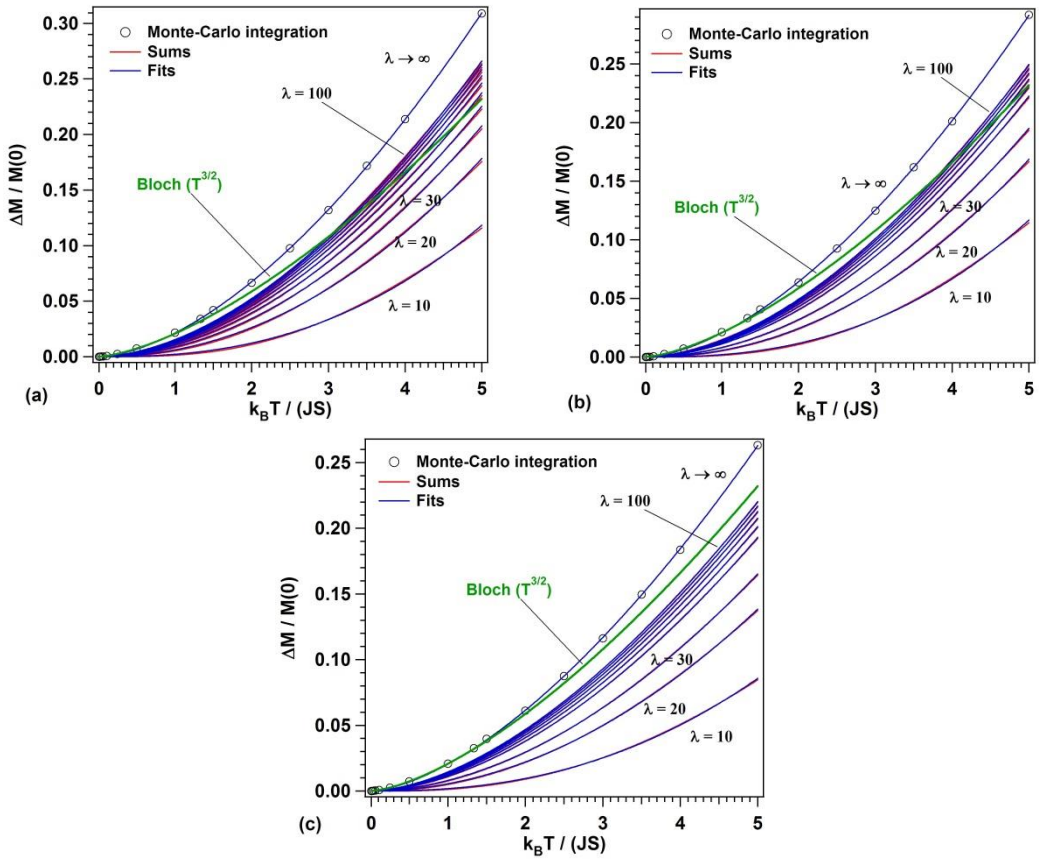

Fig. 1. Integrals of the Bose-Einstein distribution function over the first Brillouin zone for (a) simple cubic; (b) bcc structure; (c) fcc structure, together with the Bloch law (11). The blue curves represent exact sums over the corresponding finite structures, according to eq. (7), together with fits with Bloch-like formulas A x T$^{\gamma}$. One has considered S = 1. λ is a dimensionless parameter, expressing the maximum magnon wavelength in a units.

$$S\frac{|\Delta M|}{M(0)} \approx A \times \left(\frac{k_B T}{JS}\right)^{\gamma} \tag{12}$$

where the power γ yielded 1.586 for *fcc* structure, 1.652 for *bcc* and 1.663 for *sc*. Therefore, evaluation of the integrals over the first Brillouin zone yields considerable and perhaps measurable deviations from the Bloch $T^{3/2}$ law.

Figure 1 presents also the results of the summation by using eq. (7), in all directions from (- π/a) to (π/a) in steps of $2\pi/(\lambda a)$, for different values of the λ parameter, which may be thought as the extension of the system in any of the (x, y, z) direction. Fig. 1(a) presents the results for *sc*, Fig. 1(b) for *bcc*, and Fig. 1(c) for *fcc* structure. All data are fitted with the power law (12), and the two fitting parameters A and γ are plotted as function on the size parameter λ in Fig. 2. Then, these

dependencies are simulated with exponential decay, as mentioned also in Fig. 2. From this procedure, we may derive the theoretical relative variation of magnetization vs. temperature as function on S, J and λ. In Appendix 2, all fitting parameters from the simulations of Fig. 2 are given with an increased number of significant digits, such that one can build up the $\Delta M/M(0)$ curve quite easily for all the three crystal structures considered in this paragraph.

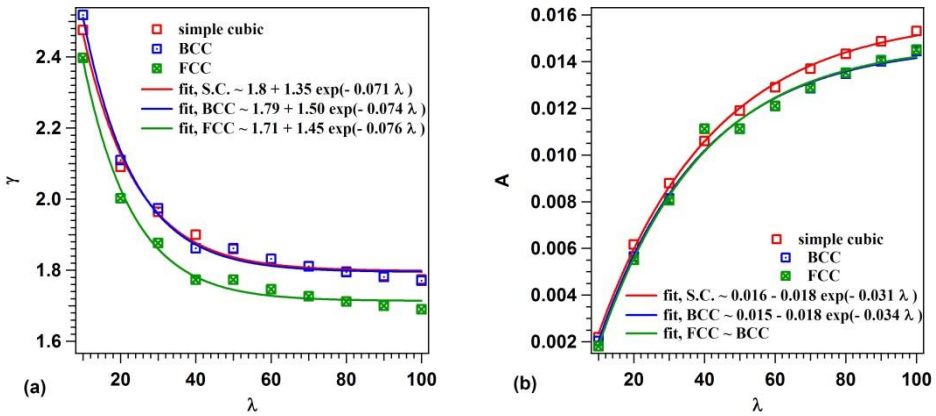

Fig. 2. Fitting parameters (A in (a) and γ in (b)) for the magnetization curves obtained for finite structures from Fig. 1, as function on the size parameter λ, together with simulations with exponential decaying functions, whose approximate formulas are given on each figure.

3.2. Two dimensional systems. Size effects

In the 2D case, the Bose-Einstein integral becomes finite only by introducing the minimum magnon wavevector cutoff $k_{\min.} = 2\pi/(a\lambda)$. In Ref. [6], an evaluation of the Bose-Einstein integral is made by introducing this cutoff (however, letting infinity for the upper integration limit), which can be translated within the actual notations as:

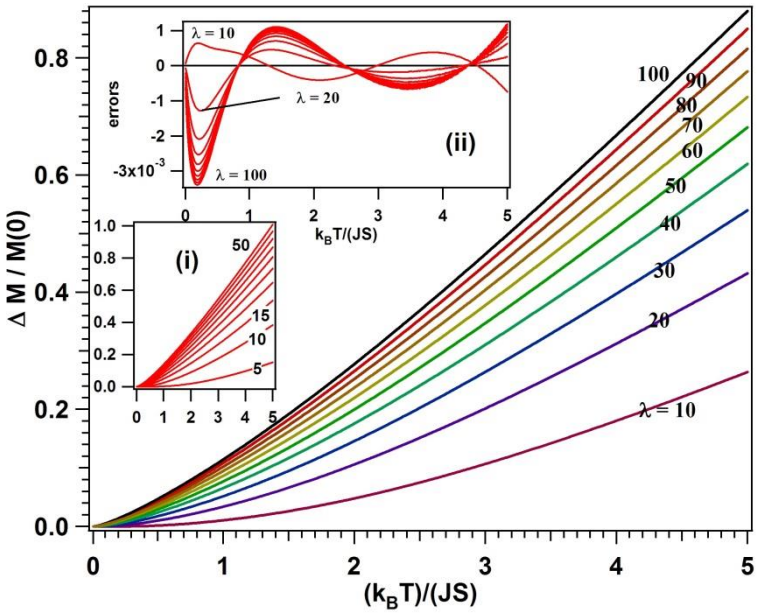

Fig. 3. Magnetization curves for 2D systems ($S = 1$), as function on the size parameter λ, by direct summation. Insert (i) presents evaluation of the integrals with cutoff parameters, eq. (13). The results of the summation from the main graph are fitted by eq. (14), and insert (ii) represents the errors of the fitting procedure, since the fits are indistinguishable from the initial computations on the graph.

$$\left(\frac{|\Delta M|}{M(0)}\right)_i(\lambda) \approx \frac{\pi}{\lambda^2 S} - \frac{k_B T}{8\pi J S^2}\log\left\{\exp\left(\frac{8\pi^2 JS}{\lambda^2 k_B T}\right) - 1\right\} \tag{13}$$

However, we found more useful to perform 2D sums for this system. Figure 3 presents the results, together with a fit of these curves with the following formula:

$$S\left(\frac{|\Delta M|}{M(0)}\right)_s(\lambda) \approx A(\lambda) \times \left\{\left(\frac{k_B T}{JS}\right) + x_0(\lambda) \cdot \exp\left(-\alpha(\lambda)\left(\frac{k_B T}{JS}\right)\right)\right\} \tag{14}$$

In one of the inserts of Fig. 3, the integral dependencies from eq. (13) are also given. Empirically, for average size systems, one finds:

$$\left(\frac{|\Delta M|}{M(0)}\right)_s(\lambda) \approx \left(\frac{|\Delta M|}{M(0)}\right)_i(\lambda/2) \tag{15}$$

which has the following explanation: the cutoff parameter introduced in evaluation the Bose-Einstein integral and yielded eq. (13) is a cutoff parameter related to the maximum radial size of the system (considered circularly symmetric), whereas the λ parameter refers to the whole system, thus its equivalent for the 'integral' system is rather the diameter of the circle in the ***k*** plane.

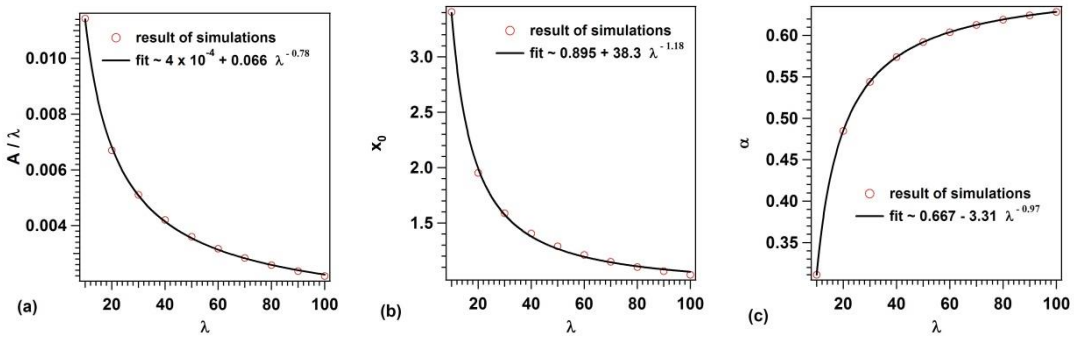

Fig. 4. Fitting parameters (A in (a), x_0 in (b) and α in (c)) for the magnetization curves obtained for finite structures from Fig. 3, as function on the size parameter λ, together with simulations by using power functions, whose approximate formulas are given on each figure.

The λ dependencies of A, x_0 and α from eq. (14) are plotted in Fig. 4. The same procedure is followed as in the previous paragraph, namely these dependencies are simulated with empirical functions (power laws, such as $a + b \times \lambda^c$), and the parameters a, b, c are fitting parameters. Rounded values of these parameters are given in Fig. 4, whereas more exact values of them are listed in Appendix 2.

3.3. One dimensional systems

The same procedure was applied for 1D summation. The same model functions are used for the fitting of the relative magnetization dependence on the temperature, and for the dependence of the fitting parameters on λ. The results are all summarized in Fig. 5. Fig. 5(a) presents the $|\Delta M(T)|/M(0)$ dependence on $k_B T/(JS)$, for several values of λ. Fig. 5(b-d) presents the dependencies of A, x_0 and α from eq. (14), together with their fits by $a + b \times \lambda^c$. The fitting parameters a, b, c are sketched in Fig. 4, more exact values are also listed in Appendix 2.

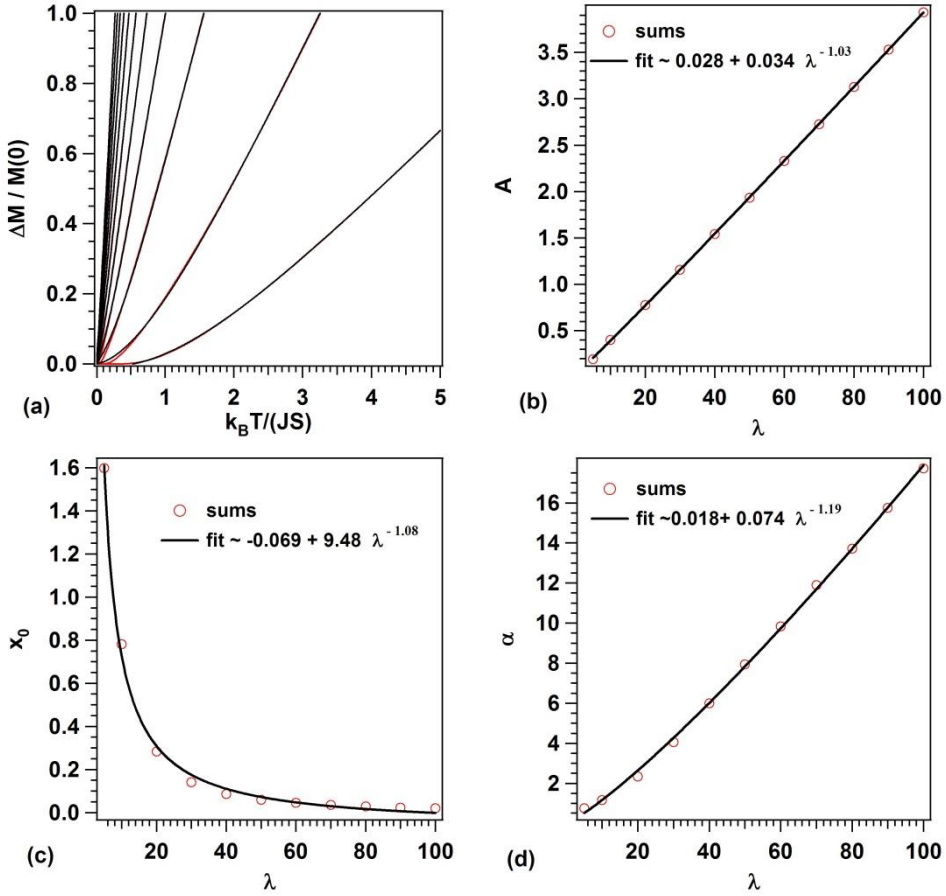

Fig.5. Results of simulations for the 1 D case: (a) relative magnetization dependence on temperature, together with its fit by eq. (14); (b-d) fitting parameters (A in (a), x_0 in (b) and α in (c)) for the $|\Delta M(T)|/M(0)$ dependences as function on the size parameter λ, together with simulations by using power functions, whose approximate formulas are given on each figure.

4. Experimental data analysis

4.1. Usefulness of the method to derive size, dimensionality, and crystal structure of finite size magnetic systems

The estimated results which may be obtained from $M(T)$ in view of the present considerations suggest that trials should be made to apply these considerations in order to derive nanoparticle or nanoisland sizes, dimensionalities, and crystal structures just from magnetometry. However, there are number of experimental limitations or side effects which will be considered in the present paragraph.

Taking into account the above observations, particularly on the magnitude of the $\Delta M(T)$, as may be derived from eqs. (12) and (14), no doubt exists that consistent experiments could be performed for 2D systems. Particularly, for larger 2D systems, the decrease in the magnetization will be more and more abrupt, although the temperature exponent approaches unity for a wider range of temperatures. The recent example of Ref. 6 proved that this method works and could provide useful information (e.g. lateral dimension of nanoislands) even for buried 2D magnetic layers.

A more serious problem occurs when one desires to investigate 3D systems, which commonly consist on magnetic nanoparticles separated in a matrix, with eventually a size distribution. We focused on the idea of determination of the size and crystal structure of such 3D

systems, where this times the relative variation of the magnetization from its value at 0 K is just a few percents. Such systems exhibit superparamagnetic (SP) behaviour [16-18], consisting in: (i) existence of a regime at higher temperatures where the magnetic spins are aligned inside the nanoparticles, but the overall nanoparticles' spins are mutually decoupled (SP); (ii) existence of a "blocked" regime at lower temperatures, whose explanation is that thermal activation is not sufficient to take over magnetic anisotropy and to promote alignment of the moments of nanoparticles with the applied magnetic field [16-19]; (iii) even in the SP regime, mutual interactions between nanoparticles are not negligible, consequently one speaks about "interacting superparamagnetic regime" (ISP), described phenomenologically by the addition of an offset in the temperature T^*, connected to random dipolar interactions between nanomagnets [20]. The blocking temperature (T_B) is usually determined from field-cooled and zero field-cooled $M(T)$ [21], or from the coercitive field dependence with temperature α $\{1 - (T/T_B)^{1/2}\}$ [19,22,23]; it is connected to the product between the magnetocrystalline anisotropy constant and the nanoparticle volume [16-19], divided by $\log(\omega_0/\omega)$, where ω_0 is a frequency related to the experimental variation of the magnetic field and ω the attempt frequency to induce magnetization reversal. The latter is connected to the ferromagnetic resonance frequency [24].

Generally, the magnetization curve $M(H)$ in the SP regime is well approximated as the Langevin function, which is used to determine the overall magnetic moment of the nanoparticle and hence its size (number of individual magnetic moments) [20]. The situation is somehow complicated when dealing with distributions of nanoparticles, where phenomenological description of their size distribution (e.g. lognorm) should be taken into account [23,25,26]. Recent studies have shown that interaction between nanomagnets could alter the derivation of the nanoparticle sizes [20], that also the magnetic anisotropy exhibit considerable dependence with temperature [22]. Up to now, in either the SP, the ISP or the blocked regime the overall saturation magnetization of nanomagnets was considered constant [22,23]. Within the present work, also this hypothesis is questionable, owing to spin waves inside the nanoparticles.

It is difficult to separate between all these effects, all of them depending on temperature. It was noticed that even for nickel, which has the weaker anisotropy of the 3*d* metals [27], blocking temperatures vary between 20 to 40 K (from an experimental study [23]) or between 50 and 150 K (theoretical study for Ni nanoparticles of 10 x 10 x 10 nm^3, respectively 20 x 20 x 20 nm^3 [22]). There are two measurement philosophies: (i) to concentrate in the SP regime, fit with the Langevin function and plot the resulting moments as function of temperature (with eventual temperature offset correction from random dipolar forces, as proposed in Ref. [20]); this is recommendable for systems with low anisotropy; (ii) to concentrate in the blocked regime and remove the Arrhenius deviation towards equilibrium, recommended for systems with high anisotropy (this could be achieved e.g. by comparing "fast" and "low" measurements etc.); (iii) to use dedicated high spatial resolution techniques, allowing experiments of a single nanoparticle / nanomagnet / nanodot, such as magnetic force microscopy, confocal Kerr microscopy [28], X-ray magnetic circular dichroism using "micro-XAS" facilities at synchrotron research centers, etc. We have suggested that experiments will give the final advice whether the method may be commonly used in 3D systems or not. However, in the following we will question several systems by the simpler approach developed above, based on magnetization curves versus temperature, in the low temperature regime.

4.2. Examples

a) Half a monolayer of Mn deposited on Cu(001), reconstructed c (2 x 2)

This experiment is reported in Ref. [29]. Half of a single Mn layer is deposited on Cu(001) and forms a well ordered superstructure *c* (2 x 2), as seen by low energy electron diffraction (LEED). That means that, in average, one Mn atom is present for each two surface unit cells of Cu(001). This surface was ferromagnetic at low temperatures, as it was probed by X-ray magnetic circular dichroism. The temperature dependence of its magnetization is plotted in Fig. 6(a).

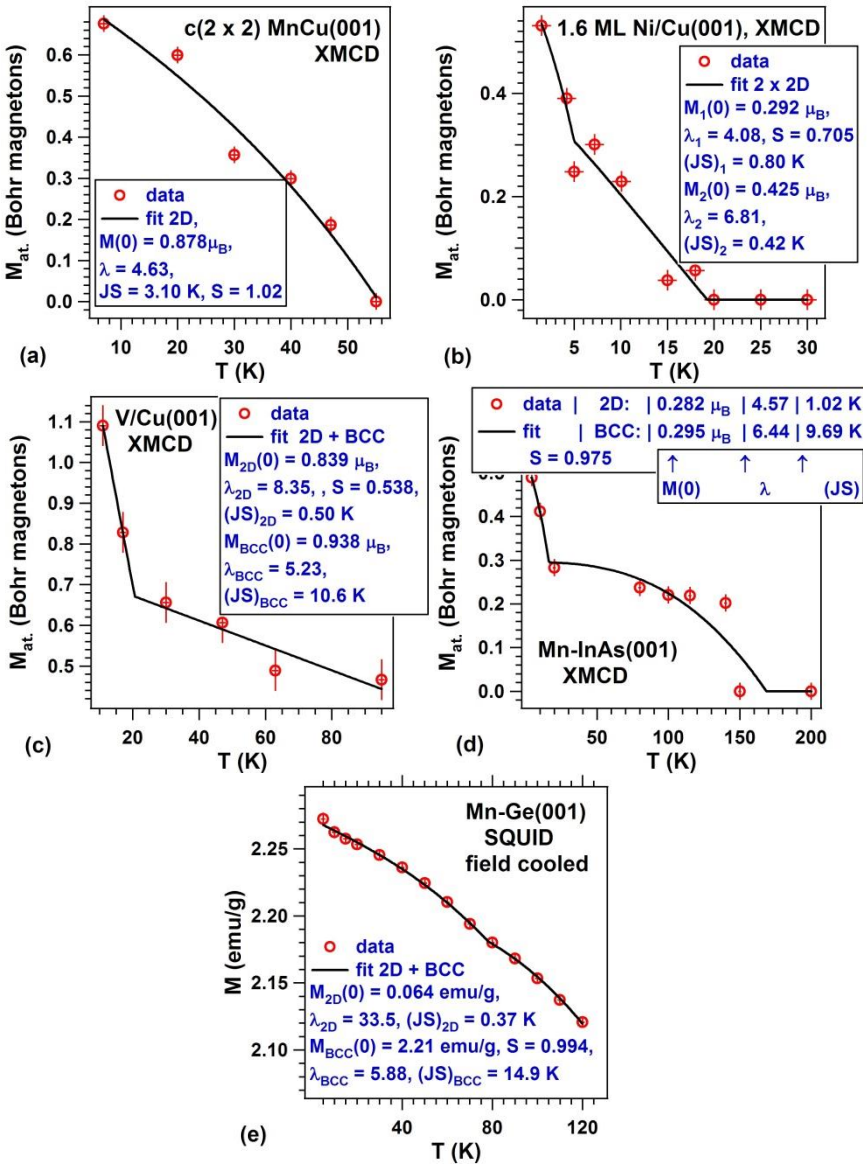

Fig. 6. Experimental data analysis: (a) MnCu(001) surface alloy [29], with one 2D phase; (b) Ni monolayer/Cu(001) [6], with a combination of two 2D phases; (c) V nanoparticles on Cu(001) [10]; (d) 2 ML Mn diluted in InAs(001) [7-9]; (e) MnGe(001) ferromagnetic alloy [31]. Cases (c-e) are simulated with one 2D and one bcc phase.

The data are well fitted with a single 2D component, yielding the zero temperature Mn magnetic moment of ~ 0.9 μ_B, the average spin quantum number ~ 1, and the exchange integral ~ 3 K. Now, normally for a spin quantum number of 1, the zero temperature magnetization should yield 2 μ_B, unless ferrimagnetism is present. In Ref. [29] it was also shown that the surface is very quickly contaminated, and extrapolating time-dependent measurements towards the preparation moment yielded an hypothetical $M(0)$ close to 2 μ_B. Therefore, the spin moment obtained, close to 1, is a realistic value and also it may point out on a consistent electron transfer toward the Cu substrate, of at least 3 electrons for each Mn atom. Also, the average island size of the Mn superstructure is rather low, $\lambda \sim 4.6$.

b) 1.5 ML of Ni deposited on Cu(001), (1 x 1) reconstruction

This second example is taken from Ref. [6] and re-analyzed in the framework of the actual considerations. The $M(T)$ dependence for 1.5 ML of Ni deposited on Cu(001) and preserving its (1 x 1) LEED pattern is represented in Fig. 6(b). Note that, according to Ref. [30], Ni forms 2D

islands buried under the first surface layer, which is occupied by Cu atoms only. Therefore, a technique such as the one we are applying now allows one to derive interesting parameters for buried layers, not available by other techniques, such as magnetic force microscopy (MFM). The experimental data are well fitted with two 2D phases with low magnetic moments (~ 0.3 and 0.4 μ_B), for an average spin value of 0.7. It may be shown that such a ratio between the magnetic moment and the average spin may come from two *ferrimagnetic* phases with configurations such as (↑↓↑) and (↑↓↑↓↑) where theoretically these rations $M(0)/(S\,\mu_B)$ should have been 2/3 (≈ 0.4/0.7) and 2/5 (≈ 0.3/0.7). The exchange integral, also, is quite low for both phases, and the average island size is similar (λ ~ 4.0 and ~ 6.8). By taking into account this average island size, a model such as represented in Fig. 7 may be proposed, with constitution of square islands with compensated spins, and addition of extra spins, which are responsible for the total magnetic moment. For instance, an island formed by 4 x 4 Ni atoms with 7 aligned extra Ni spins will produce a net moment of 14 μ_B for 23 atoms with average spin quantum number of 1, therefore the ratio between the atomic magnetic moment and the average spin is 14/23 ≈ 0.61, to be compared with 0.60 obtained from the second phase identified in Fig. 6(b). The first phase, with a ratio of the atomic magnetic moment to the average spin of 0.41, may be well simulated as a superposition of (4 x 4) cells with 3 and 4 extra atoms, where the computed ratio will be 6/22 ≈ 0.27 and 1/3 ≈ 0.33.

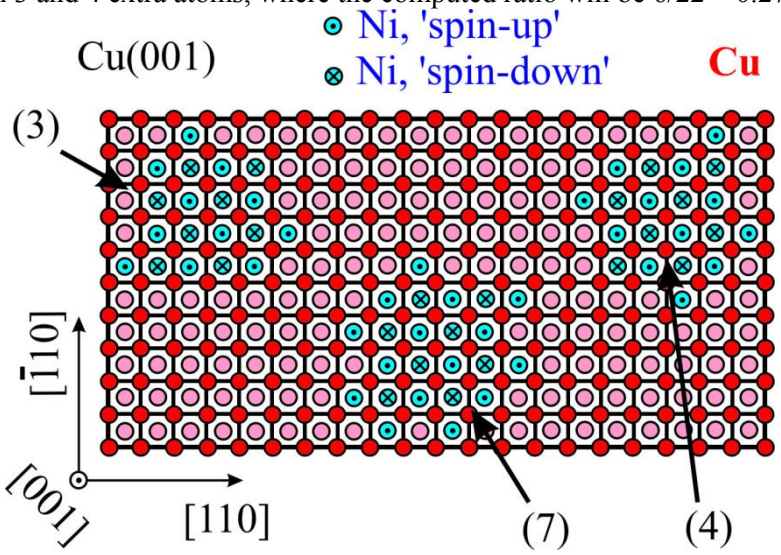

Fig.7. Model for the Ni/Cu(001) system. Three 2D islands with fully compensated Ni spins are represented, and each island has an extra number of uncompensated Ni spins, indicated with black arrows. The remaining sites are occupied by Cu atoms, since latest experimental evidence showed that at room temperature deposition Ni is buried under the first Cu single atomic layer.

c) V nanoparticles deposited on Cu(001)

These data are reported in Ref. [10]. From the $M(T)$ dependence, it was reported that this system is ferrimagnetic. In Fig. 6(c), these data are fitted with a combination of two phases, one 2D and one *bcc*. Both phases have $M(0)$ moments close to 1 Bohr magnetron, whereas the average spin is close to 0.5. This suggests rather a pure ferromagnetic behavior of both phases, composed of 2D and 3D *bcc* phases with typical sizes of 70-130 atoms. Interestingly, the number of atoms in a phase doesn't change too much from 2D to 3D. Note also that the exchange integral of the 3D *bcc* phase is much larger (about 11 K, to be compared with 0.5 K).

d) 2 ML of Mn diluted into InAs(001)

This system has been discussed in Refs. [7-9], however, without too many considerations on the origins of magnetism in Mn diluted in InAs(001). Fig. 6(d) presents this analysis and it turned out that it can be again simulated with a 2D component plus a 3D *bcc* component. (The kind of 3D component was chosen by fitting separately with different 3D components and

choosing the fit which provided the better results, i.e. the lowest value of χ^2.) Both moments are quite low for a relatively elevated value of the spin. In fact $M(0)/(S\ \mu_B)$ approaches $(2/7) \approx 0.285$, which suggest ferrimagnetism with an unit magnetic cell such as (↑↓↑↓↑↓↑).

e) A thick Mn film deposited on Ge(001) at high temperatures

This sample was produced by evaporating a thick Mn film (100 nm) onto Ge(001) held at 350 °C [31]. This system provides room temperature ferromagnetisn; also the superconducting quantum interference device (SQUID) curves exhibited differences between the field cooled and the zero field cooled $M(T)$ curves. The bigger discrepancies are at around 160 K, where a magnetic ISP transition is identified. For the actual evaluation, we used just the low temperature SQUID data obtained in the field cooled measurement. This behaviour may be simulated with two phases, one 2D and one 3D *bcc*. Interestingly, in this case the 3D aggregates contain fewer atoms (about 200) than the 2D islands (over 1,000).

As a general remark for all cases discussed in this Section, the exchange integrals obtained for 2D phases are quite low (on the order of 1 K or below, with the exception of the MnCu surface alloy, about 3 K), whereas the exchange integrals J obtained for the bulk phases are much stronger, exceeding 10 K, i.e. about 1 meV. Also, one may notice that all the Mn-based ferromagnetic or ferrimagnetic system discussed have a Mn magnetic moment at 0 K close to 1 μ_B, corresponding to a a single unpaired electron; electron transfer from manganese to its surrounding (Cu(001) surface, InAs(001) or Ge(001) crystals) cannot be excluded.

Finally, we must mention that all the analyzed data are obtained in relatively strong magnetic fields: 1 T for MnCu(001) surface alloy, 5 T for Ni/Cu(001) and for InAs(001):Mn, 7 T for V/Cu(001), with a lower magnetic field of 0.05 T for Ge(001):Mn. Therefore, we cannot speak really about ferromagnetism in these systems, but rather on the spin orientation in strong magnetic field, including superparamagnetic behavior. There are few data in literature on low dimensionality systems obtained when no magnetic field is applied, i.e. in remanence. In the case of the five systems analyzed in this paper, one cannot state that these systems are real ferromagnets. Also, one has to take into account the fact that ferromagnetism is a property of a large system, whereas the derived sizes for the actual systems are rather low. Therefore, we analyzed the dynamics of the spin orientation in an applied magnetic field and not the real ferromagnetism of these structures. It was shown that even in presence of applied strong magnetic fields, spin waves still manifest in the temperature variation of the magnetization. The magnetic interaction energy in an applied field B_a (~ 5 T) is on the order of $\mu_B B_a \sim 0.29$ meV ~ 3.3 K. This value exceeds the 'exchange integrals' derived for Ni/Cu(001), V/Cu(001)-2D and Mn:InAs(001)-2D, where 2D stands for the 2D component. Consequently, the linear slopes of these magnetization curves are due to superparamagnetism, i.e. orientation of surface spins by the applied magnetic field, rather to the exchange interaction. The only case when a surface (2D) ferromagnetic component occurs is that of c(2 x 2) MnCu(001) surface alloy, where the measurements were performed in an applied field of 1 T, therefore the maximum magnetic energy is on the order of 0.67 K, while the derived exchange integral is about 3 K. In turn, the 'bulk' components derived for V/Cu(001) and for the two cases of Mn diluted in semiconductors, whose exchange integrals exceed 10 K, represent real ferromagnetic behavior. Moreover, the considerations from the present paper allows one to extract spin configurations (e.g. such as the ones represented in Fig. 7) even for finite systems in presence of applied magnetic fields, without ferromagnetism. The spin wave theory is applicable, no matter if the spins are oriented by the exchange interaction or by an applied external field.

5. Conclusions

Monte-Carlo evaluation of integrals over Bose-Einstein distribution functions have been performed, by using exact magnons' dispersion laws for *sc*, *bcc*, and *fcc* lattices for bulk 3D systems, and we found that the $M(T)$ law deviates from the Bloch $T^{3/2}$ law. The deviation depends

on the crystal structure. The temperature exponent varies between 1.59 for *fcc* to 1.66 for *sc* and *bcc*. The case of low size 3D nanoparticles is treated by evaluation of the sum over all possible magnon wavevectors, by taking into account that their eigen values are quantified $k_{x,y,z} = 2\pi n_{x,y,z}/(a\lambda)$, where λ is the nanoparticle size along any of the three axes and $n_{x,y,z}$ ranges from $-\lambda/2$ to $+\lambda/2$. More drastically deviations from the Bloch law are obtained for nanoparticles: the temperature exponent can increase up to 2.5 for $\lambda = 10$. Again, the $M(T)$ law depends on the crystal structure considered for these nanoparticles.

For lower dimensionality (2D and 1D) the sum over magnons states of the Bose-Einstein distribution function yields a finite result only for finite size systems. The $M(T)$ behavior is obtained by direct summation and compared with evaluations by using integrals with a lower wavevector cutoff [6]. All the 3D, 2D and 1D computations are simulated with analytical functions, such that a direct dependence of $M(T)$ may be obtained by using as input values the size of the system λ, the average spin S, and the exchange integral J. These formulas are useful to identify the size, dimensionality and some relevant parameters (S, J) for magnetic systems composed by finite nanoparticles. J is not necessarily the ferromagnetic exchange integral, but can also be thought as the interaction energy with an applied external magnetic field.

After a critical review of the feasibility of the experiments and of the reliability of the data interpretation, some recent practical data are discussed, allowing one to derive more details about the size, interactions and magnetic properties of systems with finite dimensions and variable dimensionality.

Acknowledgements

This work is supported by the PN2-Partenerships 152/2011 UEFISCDI and by the Kernel Programme of the National Institute of Materials Physics, Project No. PN06-410101.

References

[1] C. Kittel, *Introduction to Solid State Physics*, Fourth Edition, John Wiley & Sons, New York (1971).
[2] N.D. Mermin and H. Wagner, Phys. Rev. Lett. **17,** 1133 (1966).
[3] M. Kollar, I. Spremo, P. Kopietz, Phys. Rev. B **67**, 104427 (2003).
[4] F.J. Dyson, Phys. Rev. **102**, 1217 (1956); *ibid.* 1230 (1956).
[5] S.V. Maleev, Sov. Phys. JETP **64**, 654 (1958).
[6] C.M. Teodorescu, Surf. Sci. **601**, 4292 (2007)
[7] K. Hricovini, P. De Padova, C. Quaresima, P. Perfetti, R. Brochier, C. Richter, V. Ilakovac, O. Heckmann, L. Lechevallier, P. Bencok, P. Le Fevre, C. Teodorescu, Appl. Surf. Sci**.** **17**, 212 (2003).
[8] M.C. Richter, P. De Padova, C. Quaresima, P. Perfetti, R. Brochier, V. Ilakovac, O. Heckmann, L. Lechevallier, M. Zerrouki, C. Teodorescu, C.S. Fadley, N. Hamdan, K. Hricovini, J. Alloys Compds. **41**, 362 (2004).
[9] C. M. Teodorescu, M. C. Richter, K. Hricovini, J. Optoelectron. Adv. Mater. **8**, 1200 (2006).
[10] Y. Huttel, G. van der Laan, C.M. Teodorescu, P. Bencok, S.S. Dhesi, Phys. Rev. B **67**, 052408 (2003).
[11] P. Crespo, J.M. Gonzalez, A. Hernando, F.J. Yndurain, Phys. Rev. B **69,** 012403 (2004).
[12] S. Cojocaru, Solid State Commun. **151**, 1780 (2011).
[13] J. Morkowski, in *Elements of Theoretical Magnetism*, S. Krupička and J. Šterberk (eds.), Academia, Prague, 35, (1968).
[14] T. Holstein, H. Primakoff, Phys. Rev. **58**, 1098 (1940).
[15] W.S. Hulscher, Thin Solid Films **9**, 377 (1972).

[16] L. Néel, Ann. Geophys. (CNRS) **5,** 99 (1949).
[17] C.P. Bean and J.D. Livingston, *Superparamagnetism*, suppl. J. Appl. Phys. **30**, 120S (1959).
[18] J.M.D. Coey, J. Appl. Phys. **93,** 8224 (2003).
[19] M.E. McHenry, S.A. Majetich, J.O. Artman, M. DeGraef, S.W. Stanley, Phys. Rev. B **49,** 11358 (1994).
[20] P. Allia, M. Coisson, P. Tiberto, F. Vinai, M. Knobel, M.A. Novak, W.C. Nunes, Phys. Rev. B **64,** 144420 (2001).
[21] M.F. Hansen and S. Morup, J. Magn. Magn. Mater. **203,** 214 (1999).
[22] C. de Julián Fernández, Phys. Rev. B **72,** 054438 (2005).
[23] F.C. Fonseca, G.F. Goya, R.F. Jardim, R. Mucillo, N.L.V. Carreño, E. Longo, E.R. Leite, Phys. Rev. B **66,** 104406 (2002).
[24] S.M. Bhagat and P. Lubitz, Phys. Rev. B **10,** 179 (1974).
[25] R. Berger, J.C. Bissey, J. Kliava, H. Dambric, C. Estournes, J. Magn. Magn. Mater. **234,** 535 (2001).
[26] O. Pana, C.M. Teodorescu, O. Chauvet, C. Payen, D. Macovei, R. Turcu, M.L. Soran, N. Aldea, L. Barbu, Surf. Sci. **601**, 4352 (2007).
[27] E.P. Wohlfarth, *Iron, Cobalt and Nickel*, North Holland, Amsterdam, 1-70 (1980).
[28] A. Laraoui, V. Halte, M. Vomir, J. Venuat, M. Albrecht, E. Beaurepaire, J.Y. Bigot, Eur. Phys. J. D **43,** 251-253 (2007).
[29] Y. Huttel, C.M. Teodorescu, F. Bertran, G. Krill, Phys. Rev. B **64**, 094405 (2001).
[30] T.C.Q. Noakes, P. Bailey, G. van der Laan, Phys. Rev. B **67**, 153401 (2003).
[31] G.A. Lungu, L.E. Stoflea, L.C. Tănase, I.C. Bucur, N. Răduţoiu, F. Vasiliu, I. Mercioniu, V. Kuncser, C.M. Teodorescu, Materials **7**, 106 (2014).

Appendix 1: *The basics of the spin wave theory [1] and the first approximation used in the derivation*

The Heisenberg Hamiltonian - $2J\,\Sigma_j\, \boldsymbol{S}_j \cdot \boldsymbol{S}_{j+1}$, by taking into account only nearest-neighbor spin interaction, suggest the following exchange magnetic field term acting on one spin from a chain $\boldsymbol{S}_j$:

$$\boldsymbol{B}_j = -2J\,\frac{\boldsymbol{S}_{j-1} + \boldsymbol{S}_{j+1}}{g\mu_B} \tag{A1}$$

such that the corresponding energy is $-\boldsymbol{\mu}_j \cdot \boldsymbol{B}_j = -g\mu_B\, \boldsymbol{S}_j \cdot \boldsymbol{B}_j$. ($\boldsymbol{\mu}_j$ is the magnetic moment of spin $\boldsymbol{S}_j$, g the gyromagnetic ratio, and μ_B the Bohr magneton). The time variation of the kinetic moment $\hbar\boldsymbol{S}_j$ is given by:

$$\hbar\,\frac{\partial \boldsymbol{S}_j}{\partial t} = \boldsymbol{\mu}_j \times \boldsymbol{B}_j \tag{A2}$$

By expressing the magnetic moment $\boldsymbol{\mu}_j = -g\mu_B\, \boldsymbol{S}_j$ and the exchange magnetic field $\boldsymbol{B}_j$ into (A2) and writing on the three components x, y, z one obtains the following system of non-linear equations:

$$\begin{cases} \dfrac{\partial S_j^{(x)}}{\partial t} = \dfrac{2J}{\hbar}\left[S_j^{(y)}\left(S_{j-1}^{(z)} + S_{j+1}^{(z)}\right) - S_j^{(z)}\left(S_{j-1}^{(y)} + S_{j+1}^{(y)}\right)\right] \\ \dfrac{\partial S_j^{(y)}}{\partial t} = \dfrac{2J}{\hbar}\left[S_j^{(z)}\left(S_{j-1}^{(x)} + S_{j+1}^{(x)}\right) - S_j^{(x)}\left(S_{j-1}^{(z)} + S_{j+1}^{(z)}\right)\right] \\ \dfrac{\partial S_j^{(z)}}{\partial t} = \dfrac{2J}{\hbar}\left[S_j^{(x)}\left(S_{j-1}^{(y)} + S_{j+1}^{(y)}\right) - S_j^{(y)}\left(S_{j-1}^{(x)} + S_{j+1}^{(x)}\right)\right] \end{cases} \tag{A3}$$

Approximation Ap1: *Small amplitude spin waves*

For small excitations $S_j^{(x,y)} << S_j^{(z)} \approx S$, S being the absolute value of the spin, the system (A3) can be written as:

$$\begin{cases} \dfrac{\partial S_j^{(x)}}{\partial t} = \dfrac{2JS}{\hbar}\left[2S_j^{(y)} - S_{j-1}^{(y)} + S_{j+1}^{(y)}\right] \\ \dfrac{\partial S_j^{(y)}}{\partial t} = -\dfrac{2JS}{\hbar}\left[2S_j^{(x)} - S_{j-1}^{(x)} + S_{j+1}^{(x)}\right] \\ \dfrac{\partial S_j^{(z)}}{\partial t} = 0 \end{cases} \tag{A4}$$

By looking for plane wave solutions of (A4) on the form $S_j^{(x,y)} = (u,v) \times \exp[i(jka-\omega t)]$, one obtains an homogenous system for u and v. This system has non-vanishing solutions provided the following secular equation is satisfied:

$$\begin{vmatrix} i\omega & \dfrac{4JS}{\hbar}(1-\cos ka) \\ -\dfrac{4JS}{\hbar}(1-\cos ka) & i\omega \end{vmatrix} = 0 \tag{A5}$$

The dispersion law for magnons follows from solving the secular eq. (A5):

$$\hbar\omega = 4\,JS\,(1 - \cos ka) \tag{A6}$$

The solution of system (A4) yields $v = - iu$, corresponding to precession around the z axis. Equation (1) can also be considered as the magnon's dispersion law for a simple one-dimensional (1D) lattice.

Appendix 2: *Dependence of the parameters of the magnetization curves on the size parameter λ.*

3D case

Simulations (Fig. 2) $(A,\gamma) = a_{A,\gamma} - b_{A,\gamma} \exp(- c_{A,\gamma}\lambda)$

Table A.2.1.

Structure	*sc*	*bcc*	*fcc*
a_A	0.0159475	0.0147378	0.0148048
b_A	0.0185389	0.0178654	0.0182782
c_A	0.0310035	0.0341797	0.0342101
a_γ	1.79749	1.79478	1.71348
b_γ	1335284	1.4999	1.45417
c_γ	0.010155	0.0740162	0.0764983

Low D case

Simulations (Fig. 4, 5(b-d)): $(A, x_0, \alpha)\,(\lambda) = a_{A, x_0, \alpha} + b_{A, x_0, \alpha} \times \lambda^{\,c_{A, x_0, \alpha}}$

Table A.2.2.

Case	2D	1D
a_A	0.000406707	0.0284886
b_A	0.0659214	0.0337071
c_A	-0.777788	1.03173
a_{x_0}	0.8949	-0.0690785
b_{x_0}	38.3496	9.48488
c_{x_0}	-1.18523	-1.07531
a_α	0.666638	0.018149
b_α	-3.31232	0.0735865
c_α	-0.969219	1.19249